BBA - Biomembranes 1866 (2024) 184236

Contents lists available at ScienceDirect

BBA - Biomembranes

journal homepage: www.elsevier.com/locate/bbamem

Quantitative live imaging reveals a direct interaction between CD44v6 and MET in membrane domains upon activation with both MET ligands, HGF and internalin B

Ryshtee Mary Tannoo [a,b], Ludovic Richert [a,*], David Koschut [b,c], Nario Tomishige [a], Sven Máté Treffert [b], Toshihide Kobayashi [a], Yves Mély [a,*], Véronique Orian-Rousseau [b,*]

[a] Laboratory of Bioimaging and Pathologies (LBP), University of Strasbourg (UNISTRA), France
[b] Institute of Biological and Chemical systems-Functional Molecular Systems (IBCS-FMS), Karlsruhe Institute of Technology (KIT), Germany
[c] Disease Intervention Technology Lab (DITL), Institute of Molecular and Cell Biology (IMCB), Agency for Science, Technology, and Research (A*STAR), Singapore

ARTICLE INFO

Keywords:
CD44v6
MET
Receptor tyrosine kinases
Lipids
Live cell imaging

ABSTRACT

Deregulation of the receptor tyrosine kinase MET/hepatocyte growth factor (HGF) pathway results in several pathological processes involved in tumor progression and metastasis. In a different context, MET can serve as an entry point for the bacterium *Listeria monocytogenes*, when activated by the internalin B (InlB) protein during infection of non-phagocytic cells. We have previously demonstrated that MET requires CD44v6 for its ligand-induced activation. However, the stoichiometry and the steps required for the formation of this complex, are still unknown. In this work, we studied the dynamics of the ligand-induced interaction of CD44v6 with MET at the plasma membrane. Using Förster resonance energy transfer-based fluorescence lifetime imaging microscopy in T-47D cells, we evidenced a direct interaction between MET and CD44v6 promoted by HGF and InlB in live cells. In the absence of MET, fluorescence correlation spectroscopy experiments further showed the dimerization of CD44v6 and the increase of its diffusion induced by HGF and InlB. In the presence of MET, stimulation of the cells by HGF or InlB significantly decreased the diffusion of CD44v6, in line with the formation of a ternary complex of MET with CD44v6 and HGF/InlB. Finally, similarly to HGF/InlB, disruption of liquid-ordered domains (Lo) by methyl-β-cyclodextrin increased CD44v6 mobility suggesting that these factors induce the exit of CD44v6 from the Lo domains. Our data led us to propose a model for MET activation, where CD44v6 dimerizes and diffuses rapidly out of Lo domains to form an oligomeric MET/ligand/CD44v6 complex that is instrumental for MET activation.

1. Introduction

The receptor tyrosine kinase (RTK) MET and its ligand, the hepatocyte growth factor (HGF) have essential roles in development notably in cell growth, migration of myogenic precursor cells, and survival of epithelial cells (reviewed in [1]). In adulthood, they play an essential role in tissue regeneration as demonstrated in the liver [2]. Deregulation of MET signaling occurring upon mutation of the *MET* gene or autocrine secretion of HGF results in induction of tumorigenesis and metastasis [3]. Several partners of MET and HGF participating in the activation and signaling have been described in various contexts. Integrins, plexins, or other RTKs [4] as well as CD44v6 have been shown to augment or even control the MET/HGF activation process. CD44v6, a member of the CD44 family of transmembrane glycoproteins has been shown, in co-immunoprecipitation studies, to be part of a ternary complex together with HGF and MET [5]. This method does not, however, exclude that the binding is indirect. From a mechanistic view, the extracellular domain of CD44v6 promotes the phosphorylation of MET, while its intracellular tail participates in its downstream signaling and internalization upon HGF induction (reviewed in [6]). Moreover, a direct binding between the full-length HGF and the CD44v6 ectodomain was evidenced by different biophysical methods in solution, and HGF was found to only bind to cells expressing CD44v6 [7]. Most importantly, a peptide corresponding to a sequence found in the v6 region of CD44 and inhibiting MET activation and signaling, was shown to prevent pancreatic tumor growth and metastasis in several mouse models [8].

* Corresponding authors.
E-mail addresses: ludovic.richert@unistra.fr (L. Richert), yves.mely@unistra.fr (Y. Mély), veronique.orian-rousseau@kit.edu (V. Orian-Rousseau).

https://doi.org/10.1016/j.bbamem.2023.184236
Received 23 January 2023; Received in revised form 24 September 2023; Accepted 27 September 2023
Available online 2 October 2023

In a completely different context, CD44v6 was also shown to be involved in MET-dependent invasion of HeLa cells by *Listeria monocytogenes*, responsible for *Listeria*-induced meningitis. The primary infection of mammalian cells is organized by a minimum of two proteins found on the bacterial surface, namely internalin A and internalin B (InlB). InlB binds to MET and induces cellular processes similar to the ones stimulated by HGF [9,10]. Interestingly, internalization of beads coated by internalin B (InlB) was found to rely on the cooperation of MET and CD44v6, while downregulation or inhibition of CD44v6 blocked the InlB-mediated activation of MET [11].

The exact stoichiometry of the MET/CD44v6 complex upon HGF or InlB induction still needs to be unraveled. Other unanswered questions are whether MET and CD44v6 directly interact and how CD44v6 contributes to the formation of MET/ligand complexes in cells, thereby leading to the activation process. RTK activation relies on ligand-mediated dimerization [12] and several dimerization models have already been described [13,14]. However, none of the models could be shown to be relevant for the MET receptor. High resolution and quantitative microscopy techniques such as Förster resonance energy transfer-based fluorescence lifetime imaging microscopy (FRET-FLIM), fluorescence correlation spectroscopy (FCS), and single-molecule photobleaching showed the dimerization of MET by HGF or InlB in live cells [15,16]. However, the contribution of CD44v6 was not studied in this context.

Recently, cryo-electron microscopy (cryo-EM) demonstrated two distinct MET-related complexes. The first complex consisted of a monomer of HGF that bound a MET dimer for receptor activation, and this complex was stabilized by a second HGF monomer and heparin. The second complex is formed by a dimer of NK1, corresponding to the N-terminal domain of HGF and the first kringle domain K1, connecting a dimer of MET [17]. Of note, HGF is composed of six domains, the N-terminal domain linked to four so-called kringle (K1-K4) domains in the alpha chain and a serine proteinase domain (SPH) in the beta-chain [18]. These cryo-EM data are in line with the small-angle X-ray scattering model proposed by the group of E. Gherardi [19,20]. However, the potential presence of essential co-receptors such as CD44v6 that might contribute to the formation of these complexes, was not yet analyzed. Interactions with other proteins and with membrane lipids, such as cholesterol, sphingolipids, and gangliosides, which are involved in the lateral segregation of the bulk disordered plasma membrane into liquid-ordered (Lo) microdomains [21], may influence RTK activation. Clustering of proteins and formation of active complexes driving signaling pathways rely on their spatial and temporal organization. Oligomerization and lateral diffusion of membrane proteins notably play a key role. In this context, the influence of membrane domains on MET/CD44v6 complex formation has never been explored before.

Given the importance of the MET/CD44v6 interplay in pancreatic cancer and in *Listeria* invasion, it is essential to characterize the organization and interaction dynamics of MET/CD44v6 complexes at the plasma membrane. Using FRET-FLIM, we showed for the first time, a direct interaction between MET and CD44v6 upon induction by HGF or InlB in live cells. Using FCS, we further demonstrated that HGF and InlB promoted the dimerization and increased the diffusion rate of CD44v6. Interestingly, disruption of Lo domains by methyl-β-cyclodextrin (MβCD) led to a similar increase in CD44v6 mobility. A slower diffusion was however observed for the complex MET/HGF/CD44v6. Therefore, we propose a model where HGF or InlB induces the dimerization of CD44v6 and the complex likely moves outside of confined Lo domains. The CD44v6/ligand complex then interacts with MET to create an active signaling complex.

2. Results

2.1. Interaction of MET with CD44v6 upon ligand induction

To investigate whether HGF and InlB could induce a direct interaction between MET and CD44v6, we performed FRET-FLIM experiments on T-47D breast cancer cells. FRET implies a transfer of energy from a donor dye in a non-radiative manner by direct dipole-dipole interaction to an acceptor dye. It occurs when the two fluorophores are within 10 nm and with substantial overlap between the fluorescence emission spectrum of the donor and the absorption spectrum of the acceptor (reviewed in [22]). Hence, to measure FRET, the choice of the FRET pair is decisive. To study the interaction between MET and CD44v6, we chose a FRET pair consisting of EGFP and mCherry.

The FLIM approach measures the fluorescence lifetime decay of EGFP at each pixel of an image, which is independent of the fluorophore concentration. The lifetime of EGFP is constant amidst different cells if they are in the same local environment. Hence, this method can robustly quantify FRET events, by yielding 2–3 times smaller inaccuracies compared to other FRET techniques [23]. T-47D cells do not express MET [24], which is a key advantage for the study of protein-protein interactions by microscopy techniques since interactions between non-tagged endogenous proteins and tagged proteins do not interfere with our measurements. In order to monitor EGFP lifetime at the membrane, cells were either transfected with GPI-EGFP or with MET-EGFP, the latter being used as a FRET donor. To study MET activation, it is essential to control the expression since its overexpression can lead to HGF-independent MET phosphorylation [25]. To this aim, we used an inducible gene expression system controlled by the antibiotics coumermycin and novobiocin [16,26] confirming increased HGF-induced MET activation upon CD44v6 co-transfection (Fig. S1). For the MET-EGFP fusion protein, the EGFP lifetime was 2380 ± 40 ps, which did not significantly differ from the lifetime of GPI-EGFP (2310 ± 10 ps) (Fig. 1). When MET-EGFP was co-transfected with CD44v6-mCherry, a slight but significant decrease in the lifetime was observed (2240 ± 80 ps), as a result of FRET between the two fluorophores.

To investigate the association of the two proteins during MET activation, the co-transfected cells were individually measured prior to, and after, induction with HGF or InlB. The lifetime distribution of MET-EGFP shifted toward shorter values in the presence of the ligands (Fig. 1A & B), evidencing the formation of a ternary complex between MET, CD44v6, and the ligands. Of note, a control experiment using GPI-EGFP and CD44v6-mCherry did not result in FRET, ruling out an accidental interaction between MET and CD44v6 (Fig. S2). To take into account the coexistence of bound and free MET-EGFP populations, we then analyzed the fluorescence decays with a two-component model: $F(t) = \alpha_1 e^{-\tau 1} + (1-\alpha_1)e^{-\tau 2}$, where the long-lived lifetime τ_2 was fixed at the lifetime of MET-EGFP expressed alone (2400 ps), while the short component τ_1 and its population α_1 were allowed to float. This analysis showed an increase in the fraction of bound MET from approximately 10–15 % to 30 % after ligand induction in live cells (Fig. 1C).

In order to test whether the interaction between MET and CD44v6 [5,8] is specific to this isoform, we used CD44standard (CD44s), the smallest CD44 isoform expressing no variant exon product in the extracellular domain, as a control. Using the same technique, we evaluated the interaction of MET with CD44s. In T-47D cells co-transfected with MET-EGFP and CD44s-mCherry, the MET-EGFP lifetime was observed to be at 2170 ± 90 ps. Although we observed no significant change in the lifetime distribution and fraction of interacting proteins in the presence of HGF and InlB, there was a small reduction in MET-EGFP lifetime (Fig. 2), suggesting a potential interaction between a small proportion of CD44s and MET proteins. Altogether, these data show that CD44v6 directly interacts with MET upon activation by HGF or InlB in live cells.

2.2. Binding of MET ligands to CD44v6

Using a combination of biophysical methods and pull-down assays, we had previously demonstrated a direct binding of full length HGF to the ectodomain of CD44v6 in solution [7]. Using microscale thermophoresis, we herein showed that the K4-SPH domains of HGF bound

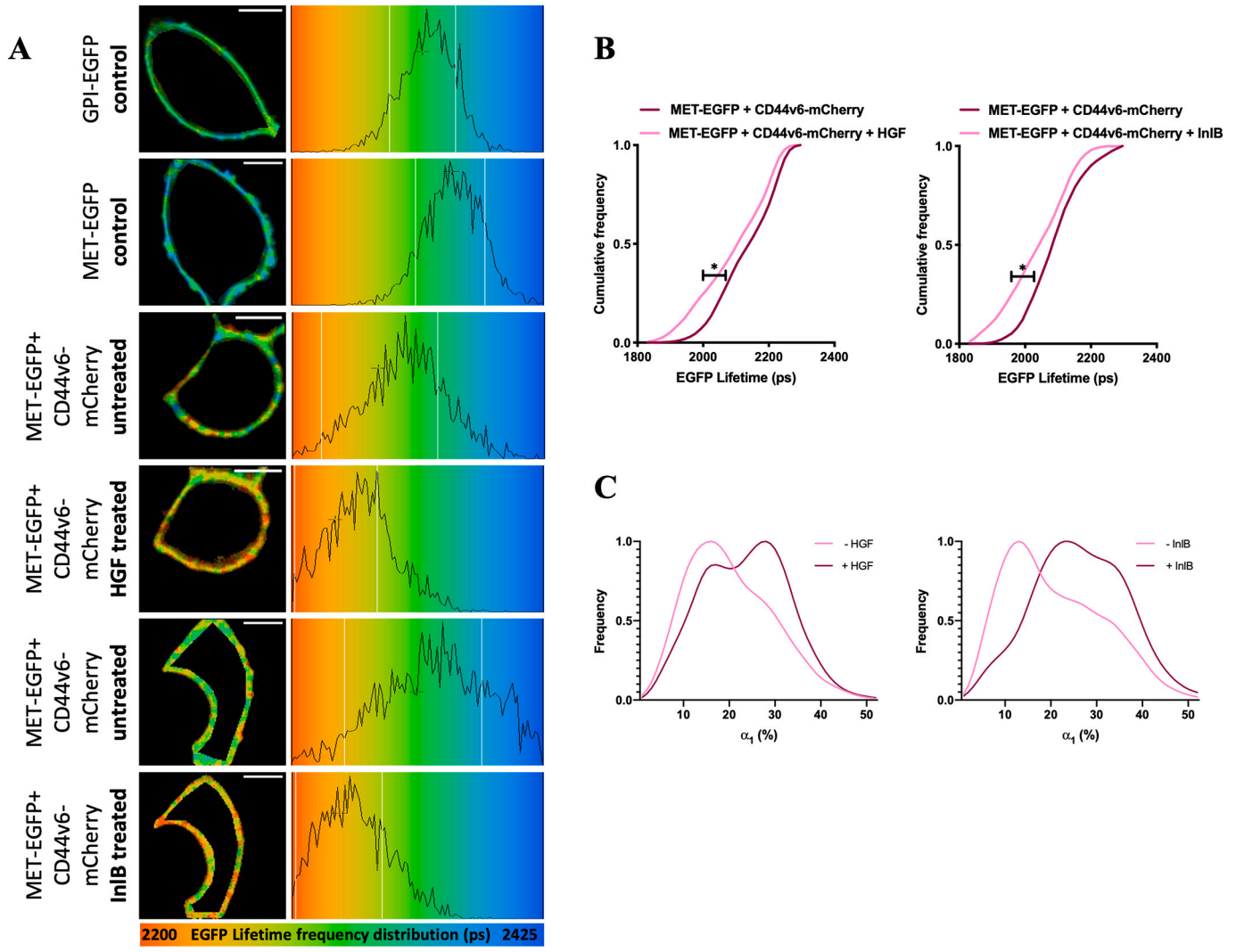

Fig. 1. Interaction between MET and CD44v6 upon ligand induction. T-47D cells were transfected with the inducible pF12A-MET-EGFP vector, the regulator pReg, and CD44v6-mCherry (1:1:1 ratio). Expression of MET was induced for 6 h with 0.8 nM coumermycin A1 and then stopped using 5 μM novobiocin. The plasmids were incubated for 24 h. Serum-starved cells were induced for 10 min with 50 ng/mL of HGF or InlB, where indicated. Fluorescence decays of MET-EGFP were recorded by FLIM and analyzed with a two-component fit using the software SPCImage (Becker & Hickl). (A) Representative color-coded images and histograms of EGFP lifetime distribution for each condition. Scale bar represents 8 μm. (B) Cumulative distributions of EGFP lifetime. A non-parametric Kolmogorov-Smirnov statistical test was performed. * = $p < 0.1$. (C) Frequency distribution of the percentage ($\alpha 1$) of MET-EGFP species interacting with CD44v6-mCherry. In the two-component fit, the free MET-EGFP proteins have a fixed lifetime of 2400 ps, while the interacting FRET species have lifetimes between 1000 ps and 2000 ps.

specifically to the CD44v6 ectodomain with higher affinity than CD44s, while the NK2 fragment of HGF showed no binding to either CD44v6 or CD44s (Fig. S3). With the same method, we further demonstrated that $InlB_{321}$, a truncated version of the bacterial MET ligand, also bound to CD44v6 with a micromolar affinity but not to CD44s (Fig. S4).

Since both HGF and InlB can induce MET dimerization [15,16,27,28], we next studied the impact of HGF and InlB on CD44v6 oligomerization using FCS, a technique which monitors the intensity fluctuations of fluorescent species diffusing through the small volume created by a focused laser beam. The dimerization of CD44v6-mCherry proteins can be deduced from the analysis of the brightness distribution of the tagged CD44v6 species diffusing through the two-photon excitation volume. The brightness varies linearly with the number of proteins within the diffusing oligomers [29–31]. By comparing the brightness of CD44v6-mCherry proteins or complexes with that of cytoplasmic monomeric mCherry proteins in transfected T-47D cells, we found that CD44v6-mCherry proteins displayed a monomeric distribution (Fig. 3A) with a low dimer population of 11 ± 1 % (Fig. 3D). CD44v6-mCherry proteins were also compared to mCherry-Mem, a cytoplasmic membrane marker containing residues of neuromodulin, which showed a dominant monomeric distribution with only 13.4 ± 2 % dimers formed. When cells were induced with MET ligands, we observed a significant increase in the population of CD44v6 dimers (Fig. 3A), which reached 21 ± 4 % and 33 ± 6 % in the presence of HGF and InlB, respectively (Fig. 3D).

FCS measurements on T-47D cells expressing CD44s-mCherry proteins (Fig. 3B) showed that the latter exhibited mostly a monomeric distribution, with only 10.1 ± 2 % dimers in non-treated cells (Fig. 3E). Addition of HGF or InlB did not significantly increase the dimer population. A very similar picture was obtained when HGF or InlB was added to T-47D cells transfected with mCherry-Mem, which is not known to interact with HGF or InlB (Fig. 3C & F). Altogether, our data showed that HGF and InlB promoted the dimerization of CD44v6 as for the MET receptor.

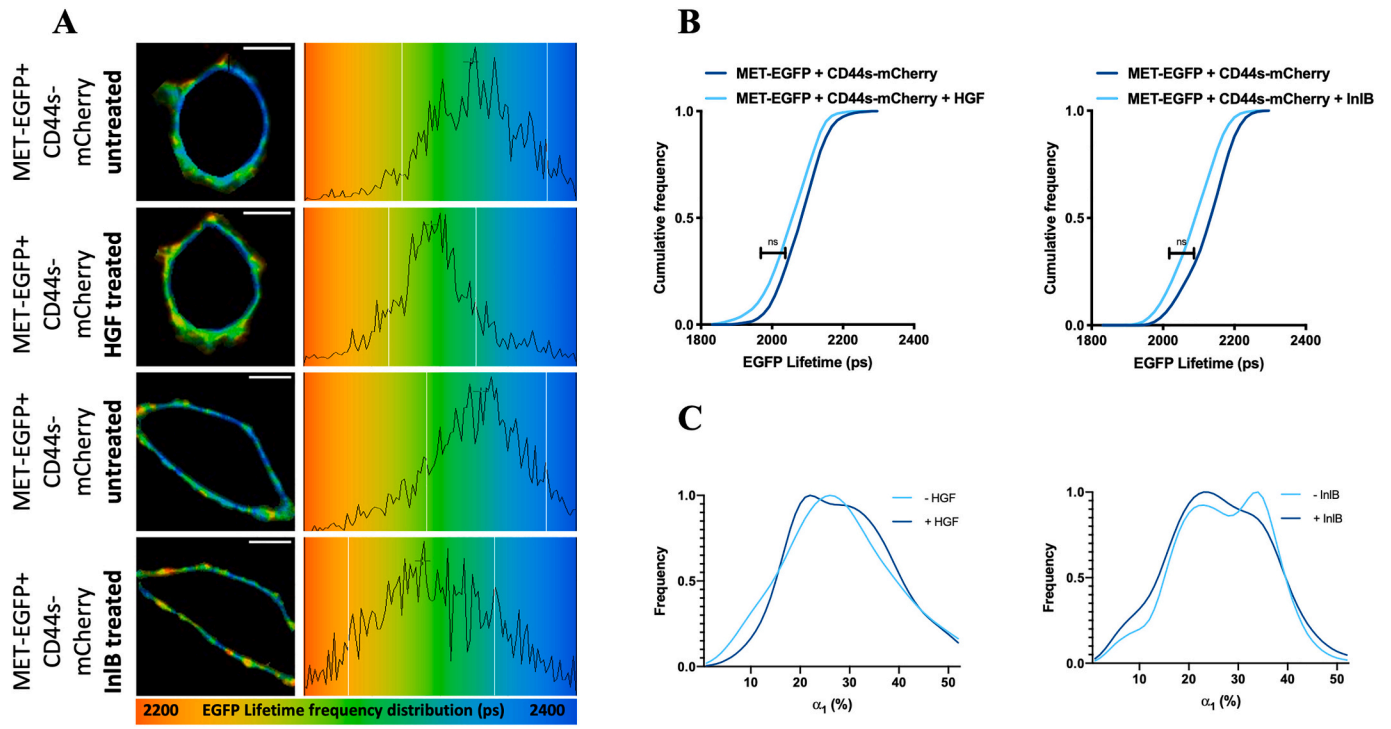

Fig. 2. No significant interaction between MET and CD44s upon ligand induction. T-47D cells were transfected with the inducible pF12A-MET-EGFP vector, the regulator pReg, and CD44s-mCherry (1:1:1 ratio). The expression of MET was induced for 6 h with 0.8 nM coumermycin A1 and then stopped using 5 μM novobiocin. The plasmids pF12A-MET-EGFP and pReg were incubated for 24 h and CD44s-mCherry for 20 h. Fluorescence decays of MET-EGFP were recorded by FLIM and analyzed with a two-component fit using the software SPCImage (Becker & Hickl). Serum-starved cells were induced for 10 min with 50 ng/mL of HGF or InlB. (A) Representative color-coded images and histograms of EGFP lifetime distribution for each condition. Scale bar represents 8 μm. (B) Cumulative distributions of EGFP lifetimes. A non-parametric Kolmogorov-Smirnov statistical test was performed. ns = non-significant. (C) Frequency distribution of the percentage ($\alpha 1$) of interacting species between MET-EGFP and CD44s-mCherry. In the two-component fit, the free MET-EGFP proteins have a fixed lifetime of 2400 ps, while the interacting FRET species have lifetimes between 1000 ps and 2000 ps.

2.3. Dynamics of CD44v6 after complex formation with MET ligands and receptor

Oligomerization and complex formation often involve lateral diffusion of proteins at the membrane. The mobility of the MET receptor has been characterized in resting and ligand-induced cells, showing a slower diffusion after dimerization induced by HGF or InlB [28,32]. Here, we investigated the diffusion of CD44v6-mCherry in resting and ligand-induced cells by FCS. The data were fitted with a two-dimensional diffusion model suited for describing lateral diffusion in membranes.

In T-47D resting cells transfected with CD44v6-mCherry, the diffusion coefficient of the labeled CD44v6 protein was 0.95 ± 0.04 μm^2/s (Fig. 4A). Interestingly, CD44v6 mobility increased by approximately two-fold after stimulation with HGF (1.9 ± 0.06 μm^2/s) and InlB (1.6 ± 0.08 μm^2/s) (Fig. 4A). In line with its membrane location, the diffusion constant of the labeled CD44v6 protein was much lower than the cytoplasmic diffusion of mCherry proteins expressed in T-47D cells (45.4 ± 0.7 μm^2/s, data not shown) or the cytoplasmic diffusion of EGFP (50.6 μm^2/s) [33]. As CD44v6 was reported to be located in Lo domains [34,35], we hypothesized that its slow diffusion in resting cells was due to its confinement in these domains. To test this hypothesis, we used methyl-β-cyclodextrin (MβCD), a drug which removes cholesterol from the membrane, reducing the Lo domains into the liquid-disordered phase at the membrane. We first confirmed that MβCD treatment disrupted membrane Lo domains by monitoring the drastic decrease in the fluorescence lifetime of F2N12S, a probe based on 3-hydroxyflavone, highly sensitive to lipid order [36] (Fig. S5). After treating transfected cells with 10 mM MβCD, the diffusion constant of the labeled CD44v6 increased significantly (1.5 ± 0.08 μm^2/s) as compared to resting cells (Fig. 4A). When the cells were incubated with 10 mM MβCD and with HGF, CD44v6 exhibited a significantly faster diffusion (2.1 ± 0.08 μm^2/s). A similar value (1.9 ± 0.2 μm^2/s) for the diffusion coefficient of CD44v6 was obtained with 20 mM MβCD. These results supported our hypothesis that CD44v6 was originally restricted in cholesterol-enriched Lo domains and suggested that CD44v6 diffused more freely in the liquid-disordered phase upon ligand stimulation. It is noteworthy that the diffusion of CD44v6 is influenced by the actin cytoskeleton since a CD44v6 fusion protein truncated from the cytoplasmic domain and therefore not linked to the cytoskeleton [37] was faster than the full-length CD44v6 (Fig. S6). This effect was also observed in presence of actin-modulating drugs such as Latrunculin B and cytochalasin D.

To evaluate the mobility of CD44v6 in the presence of MET, cells were co-transfected with MET-EGFP and CD44v6-mCherry. In the presence of MET-EGFP, CD44v6-mCherry was found to diffuse at the same rate (1.0 ± 0.07 μm^2/s) as in the absence of MET (Fig. 4A). Stimulation of the cells by HGF significantly decreased the diffusion constant (0.65 ± 0.1 μm^2/s) of CD44v6-mCherry, in line with the formation of a ternary MET/HGF/CD44v6 complex as observed in our FRET-FLIM data. While independent findings have shown slower MET diffusion after HGF induction [27,28], in this paper we demonstrated that the complex formed by MET after HGF induction included CD44v6 as well. In order to check that HGF and InlB specifically modified the diffusion of CD44v6, T-47D cells were transfected with CD44s-mCherry and its diffusion coefficient was measured in non-treated and stimulated cells. The diffusion of CD44s (1.5 ± 0.07 μm^2/s) was not affected by HGF (1.5 ± 0.07 μm^2/s), but somewhat by InlB (1.2 ± 0.07 μm^2/s) (Fig. 4B), indicating that a small fraction of CD44s might interact with InlB.

Taken together, our FCS studies suggested that CD44v6 diffuses out of confined lipid domains upon cell induction with HGF and InlB, a step that might play a role in the presentation of these ligands to the MET

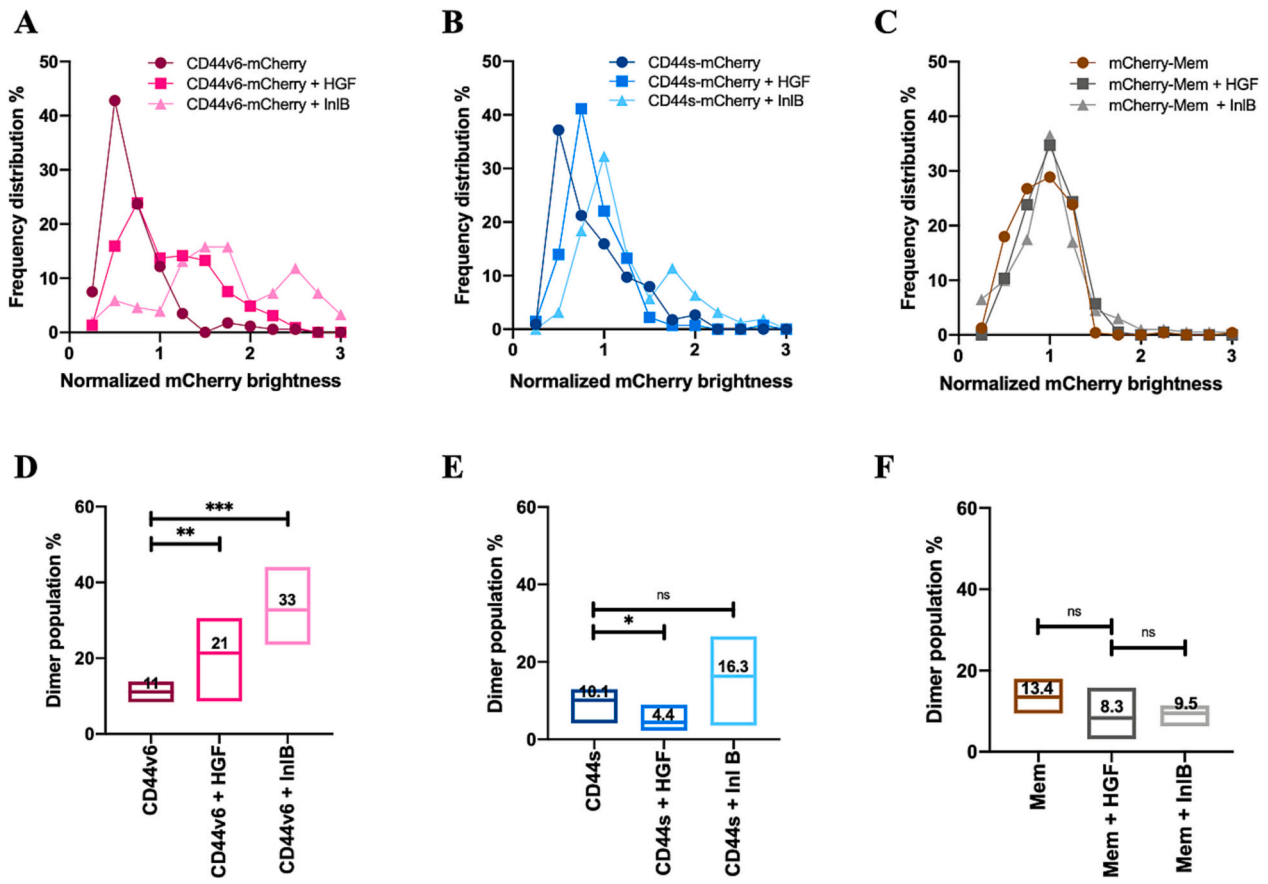

Fig. 3. CD44v6, CD44s, and mCherry-Mem dimer populations upon induction with HGF and InlB. T-47D cells were transfected with CD44v6-mCherry (A, D), CD44s-mCherry (B, E), or mCherry-Mem (C, F). Fluorescence correlation spectroscopy measurements were performed 24 h after transfection. Overall, 40 acquisitions of 5 s were carried out. Where stated, serum-starved cells were induced for 10 min with 50 ng/mL of HGF or InlB. (A, B, C) Brightness distribution of one representative experiment in each condition. The brightness was normalized to one and at least 5 cells were measured per experiment. (D, E, F) The box plots show the dimer population from at least three independent experiments, where the bottom and upper lines represent the 25 % and 75 % percentiles, respectively, and the middle line represent the annotated mean value. A one-tailed unpaired *t*-test was performed. * = $p < 0.05$, ** = $p < 0.005$, *** = $p < 0.0005$, ns = non-significant.

receptor.

2.4. Role of lipid domains in the activation and signaling of MET

To further examine the role of the membrane lipid domains in MET activation and signaling, HeLa cells were chosen since they express both MET and CD44v6 and have extensively been used for studying the RTK MET [11,38]. The cells were either left untreated or incubated with 10 mM or 20 mM MβCD, before being stimulated or not by HGF. By monitoring the phosphorylation of MET and the downstream ERK target by Western blot, we found as expected that HGF induced a strong phosphorylation in the absence of MβCD (compare the first two lanes of the gel in Fig. 5A and the two first bars of both panels in Fig. 5B). Similarly, high levels of phosphorylated MET (p-MET) and ERK (p-ERK) proteins were observed in HGF-stimulated cells treated by MβCD (Fig. 5A and B). These results were confirmed by confocal microscopy using antibodies against p-MET (Fig. 5C), as we observed a strong increase in the p-MET signal in cells stimulated by HGF, independently of the presence of MβCD (compare the three lower panels of Fig. 5C). Therefore, HGF-induced MET activation did not seem to require Lo domain integrity. Of note, we observed that MET but not ERK phosphorylation increased slightly upon MβCD treatment in the absence of HGF (Fig. 5A and B).

To confirm that cholesterol depletion did not affect MET activation, the cholesterol synthesis pathway was also inhibited. To this aim, we used two drugs, namely U18666A and lovastatin. U18666A is a cell-permeable amphiphilic amino-steroid that blocks intracellular cholesterol biosynthesis [39] and exit low-density lipoprotein (LDL)-derived cholesterol from late endosomes/lysosomes [40]. Lovastatin is a 3-hydroxy-3-methylglutaryl coenzyme A reductase inhibitor. These drugs efficiently lower the level of plasma membrane cholesterol [41] and Lo domains [42]. The phosphorylation levels of MET and ERK were not impacted by both drugs upon ligand induction (Fig. S7), confirming that MET activation by HGF might not require Lo domain integrity.

Next, we explored a possible interplay between sphingolipids and MET. Three drugs, namely myriocin (also known as ISP-1), sphingomyelinase (SMase), and desipramine were used to decrease the sphingomyelin levels by inhibiting serine-palmitoyltransferase, removing sphingomyelin from cell membranes [43,44], and decreasing the level of endogenous acid sphingomyelinase [45], respectively. HGF-induced phosphorylation of MET was not modified in treated cells compared to intact cells treated by any of these three drugs (Fig. S8). Based on the absence of effect on ligand-induced MET activity, our data led us to conclude that MET activation likely did not require Lo domains.

3. Discussion

The co-receptor function of CD44v6 for MET has been demonstrated in several primary cells and various cancer cell lines (reviewed in [46]). In pancreatic cancer in particular, the deadliest cancer, for which there is no cure, the interplay between CD44v6 and MET is decisive [8]. In several mouse models of pancreatic cancer including the KPC (*LSL-Kras$^{G12D/+}$, LSL-Trp53$^{R172H/+}$, Pdx1-Cre*) mice, inhibition of CD44v6 by a peptide blocked MET activation in the tumors and drastically

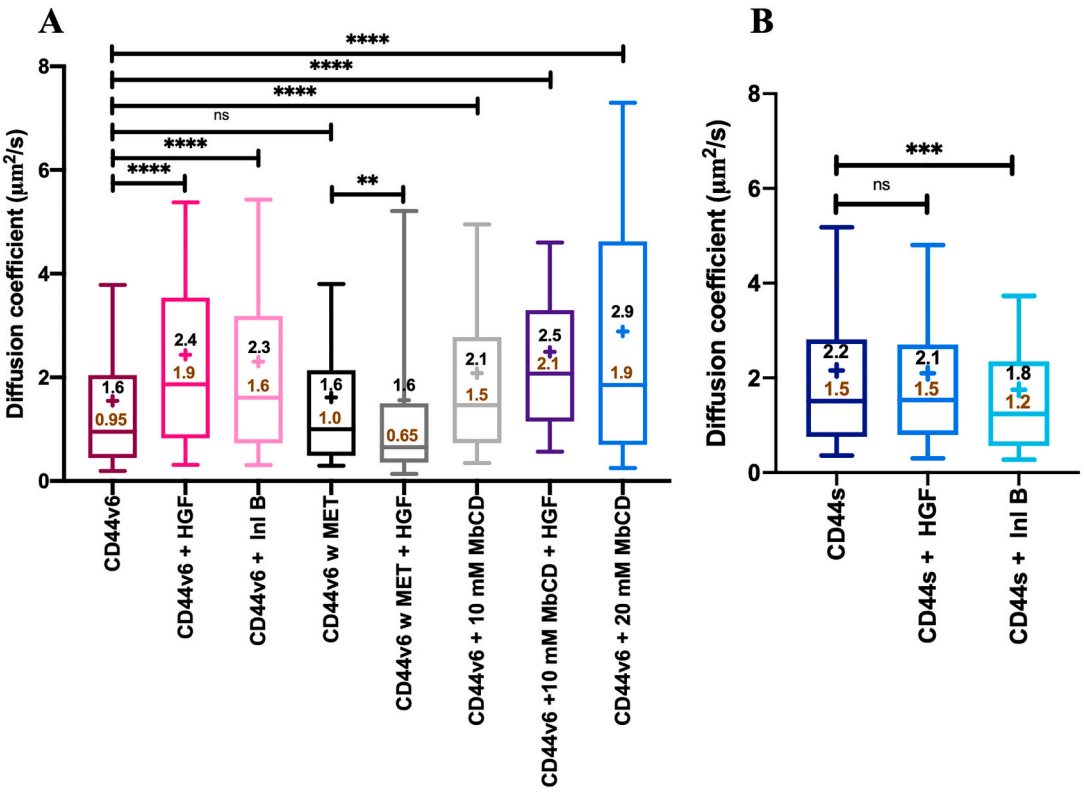

Fig. 4. CD44v6 and CD44s diffusion at the membrane. T-47D cells were transfected with (A) CD44v6-mCherry and (B) CD44s-mCherry. The diffusion of CD44v6-mCherry and CD44s-mCherry were monitored in resting cells and after stimulation for 10 min with 50 ng/mL of HGF or InlB. The effect of cell treatment with 10 mM or 20 mM MβCD for 30 min on CD44v6-mCherry diffusion was also investigated, as well as the presence of MET (w MET). The expression of MET was induced for 6 h with 0.8 nM coumermycin A1 and then stopped using 5 µM novobiocin. Fluorescence correlation spectroscopy measurements were performed 24 h after transfection and 40 acquisitions of 5 s were carried out. Diffusion coefficients were calculated from autocorrelation curves. The box plots show the median diffusion coefficients for at least three independent experiments, where the bottom and upper lines represent the 25 % and 75 % percentiles, respectively, and the middle line represent the annotated median value. The mean position is represented by a cross sign and the mean annotated in black. The error bars represent the 10–90 percentile of the data values. A Kruskal-Wallis multiple comparison test was performed. ** = $p < 0.005$, *** = $p < 0.0005$, **** = $p < 0.0001$, ns = non-significant.

decreased tumor growth and metastasis [8]. Blocking the interaction between CD44v6 and MET is therefore highly relevant. In addition to the CD44v6 peptide, other inhibitors with the appropriate pharmacokinetic and pharmacodynamic properties must be identified. To do so, a full understanding of their interaction domains and dynamics is required. In the present paper, we evidenced a direct interaction between MET and CD44v6 induced either by HGF or InlB in live cells. Moreover, our study demonstrated the binding of K4-SPH of HGF and $InlB_{321}$ to the CD44v6 ectodomain in solution (Fig. 6). Our data also showed that HGF and InlB both induced the dimerization of CD44v6 in live T-47D cells lacking MET protein expression and transfected with CD44v6 only. Finally, we demonstrated that the MET ligands induced a faster diffusion of CD44v6 similar to what we observed when depleting cholesterol from the membrane. On the other hand, the ternary complex between MET/HGF and CD44v6 diffused slower. Altogether, these data allow us to draw a model where the binding of CD44v6 to MET ligands induced the displacement of CD44v6 from the Lo structures and the formation of a ternary complex in the liquid-disordered phase of the membrane.

A recent investigation based on cryo-electron microscopy described two possible models of association between MET and HGF [17]. Within one of these complexes, one HGF molecule is enough to bridge two MET molecules and enable MET activation, while a second HGF molecule and heparin stabilize the whole structure and enhance the activation of MET [17]. Our data presented here showed a direct contact between CD44v6, an isoform which cannot be modified by heparan sulfate (HS) [5], and MET. Therefore, in our model, we suggest that the oligomerization of CD44v6 induced by HGF or $InlB_{321}$ and demonstrated in this paper, might be sufficient for stabilization of the MET/HGF complex as an alternative for heparan sulfate.

Usually, clustering of proteins relies on their lateral diffusion in the plasma membrane, which is generally reduced after oligomerization. Protein diffusion in membranes can be modulated by the actin cytoskeleton, lipid components, protein-protein interactions, or extracellular matrices. Interestingly, in our case, we observed an increase in the diffusion coefficient of CD44v6 after its dimerization by HGF or InlB. The faster lateral diffusion of CD44v6 dimers might be favorable for a rapid interaction and activation of MET. Since, similarly to HGF, removal of cholesterol by MβCD increased the diffusion of CD44v6, this suggests that cholesterol-enriched lipid domains could restrict CD44v6 mobility in untreated cells. This hypothesis is supported by a previous study reporting that CD44 proteins were partially co-localized with gangliosides (Lo domains) and with the actin cytoskeleton in KG1a cells, a human leukemic progenitor cell line [34]. Moreover, a large fraction of CD44 proteins was found to be confined or even immobile in resting macrophages [47], since they act as transmembrane pickets being restrained by the actin cytoskeleton [48]. These CD44 pickets were reported to aggregate with hyaluronan and the actin cytoskeleton to form a fence-like structure which can curtail the diffusion of other proteins such as selectins or FCγ receptors [48,49].

According to the literature, CD44v6 might be confined in Lo domains [34] and probably linked to the actin cytoskeleton [34,48,50]. Freeman et al. (2018) described a “stop and go” motion of CD44 proteins via a dynamic association and dissociation to the actin cytoskeleton. Hence, in our scenario, upon HGF or InlB induction, the CD44v6-ligand complex might dissociate from the actin cytoskeleton and diffuse out of Lo domains to enable MET activation. This hypothesis is supported by our

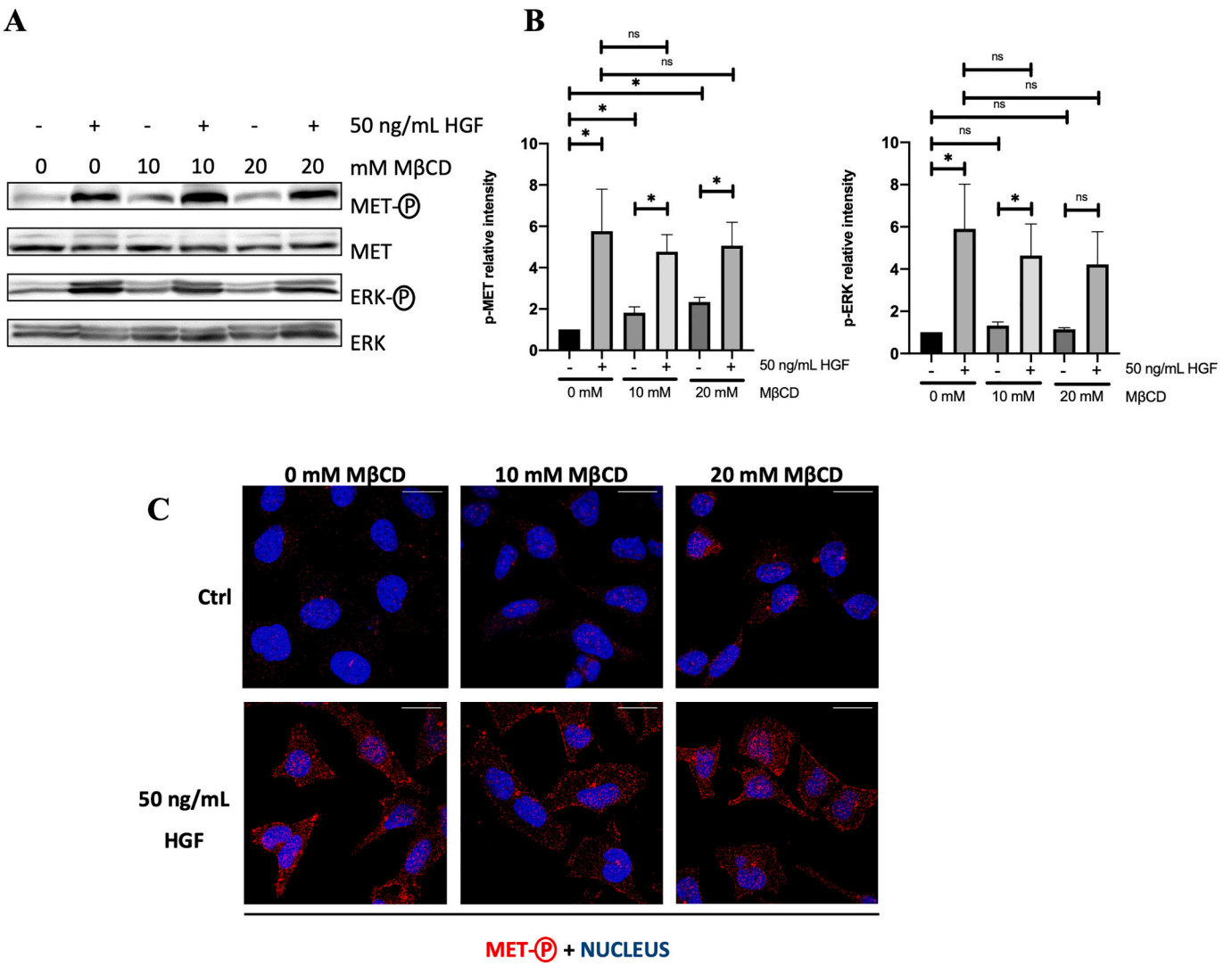

Fig. 5. Ligand-induced MET activation after incubation with methyl-β-cyclodextrin. HeLa cells were starved overnight and were incubated the next day in the absence or the presence of 10 or 20 mM MβCD for 30 min at 37 °C. Cells were then washed and induced or not with 50 ng/mL HGF for 5 min. Cells were finally lysed and subjected to Western blot analysis. (A) Phosphorylation of MET (p-MET) and ERK (p-ERK). The two proteins were detected using specific antibodies recognizing either the phosphorylated or unphosphorylated form. An unpaired t-test was carried out, * = $p < 0.05$, ns = non-significant. (B) Bar graphs representing the mean intensity of p-MET relative to MET intensity (left panel) and p-ERK relative to ERK intensity (right panel) from three different experiments. The error bars show the standard error of the mean. (C) Immunofluorescence staining was performed using antibodies against p-MET (red). The nuclei were stained with DAPI (blue). Scale bar represents 20 μm.

FCS experiment showing a faster diffusion when using a truncated version of CD44v6 in its cytoplasmic domain and/or treatment with actin-modulating drugs. Subsequently, we showed a slower diffusion of the ternary complex in agreement with the HGF-induced slower mobility of the MET protein evidenced by single particle tracking, a study which did not examine the role of CD44v6 [28]. The slower diffusion of the ternary complex is probably not directly linked to the tethering to the cytoskeleton since activation of MET in the presence of CD44v6 and HGF is independent of the cytoskeleton as shown in our previous studies [37]. However, the binding of ERM (ezrin-radixin-moesin) to CD44v6 and to the cytoskeleton is essential for MET downstream signaling and the activation of the Ras/MAPK [37,51].

It is noteworthy that HGF did not modify the diffusion coefficient of CD44s, supporting the specific interaction between HGF and CD44v6. This preferential binding of CD44v6 to HGF and InlB could be related to the much higher flexibility of the CD44v6 ectodomain over CD44s [52], which may favor a specific conformation.

Based on our data, we derived a model for the mechanism of activation of the receptor tyrosine kinase enabled by its ligands and co-receptor CD44v6 (Fig. 6 and graphical abstract). We suggest that CD44v6 proteins, which may be localized in a Lo domain, diffuses rapidly out of this domain, and dimerizes upon ligand induction. The complex HGF/CD44v6 or InlB/CD44v6 then binds MET to form a larger oligomeric MET/ligand/CD44v6 complex, diffusing at a slower rate. The formation of this complex contributes to the activation of the MET receptor, which most likely takes place in the liquid-disordered phase since we found that the phosphorylation of MET and its downstream signaling were not regulated by Lo domains. The understanding of these complex interactions between membrane proteins that are involved in tumor progression and metastasis, is essential for the identification of potential drugs blocking their function.

4. Materials and methods

4.1. Reagents

Recombinant full-length human HGF (PeproTech) was used to induce MET activation in cells. InlB prepared as explained in [53] was a

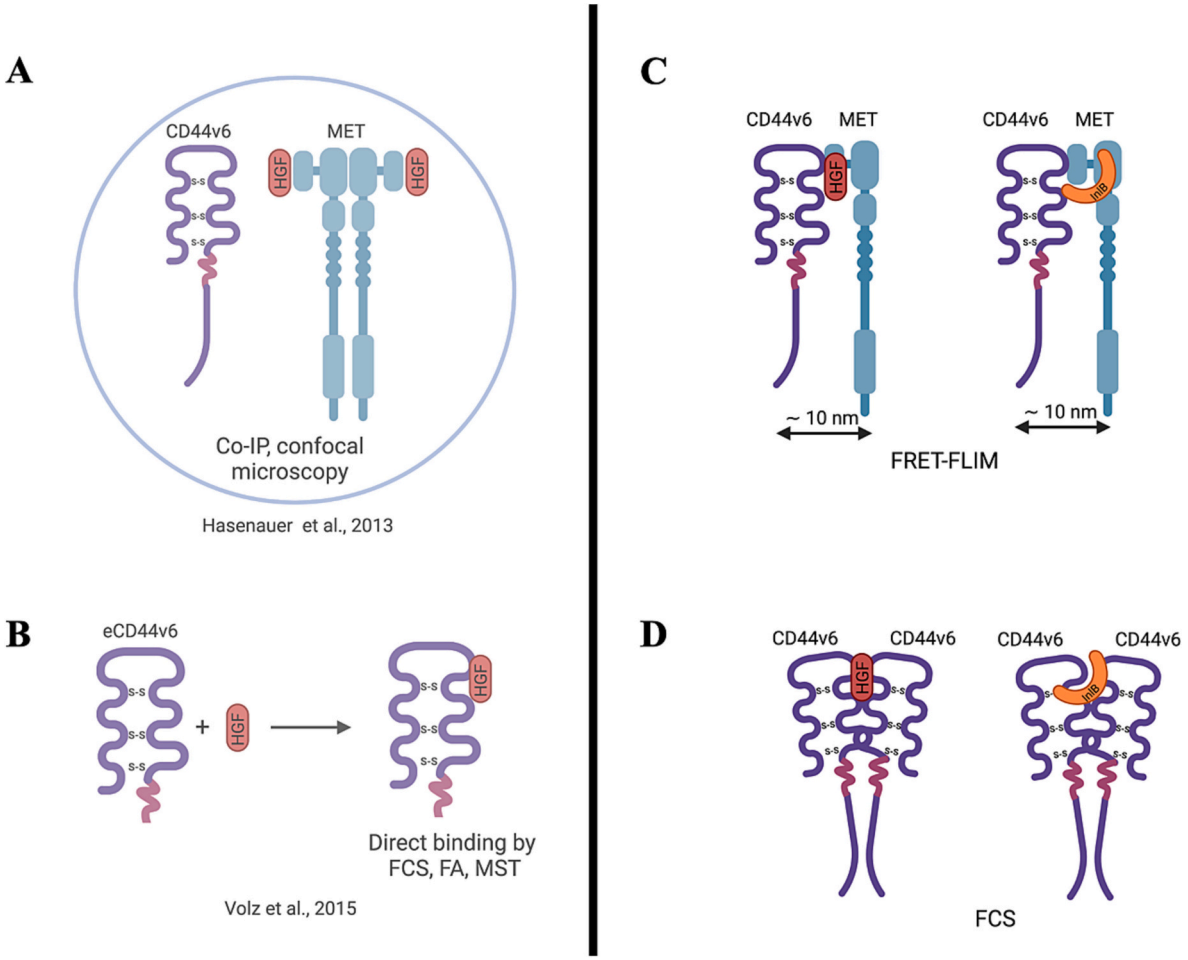

Fig. 6. Interaction of CD44v6 and MET: past and present discoveries. (A) Evidence of complex formation between MET and CD44v6 by co-immunoprecipitation (Co-IP) and colocalization by confocal microscopy (low resolution). (B) Evidence of direct binding by fluorescence correlation spectroscopy (FCS), Fluorescence anisotropy (FA), and microscale thermophoresis (MST) between the ectodomain of CD44v6 and full-length HGF in solution. (C) As evidenced by our Förster resonance energy transfer-based fluorescence lifetime imaging microscopy (FRET-FLIM) results, CD44v6 and MET interact directly in HGF and InlB-induced cells. (D) CD44v6 is dimerized in the presence of HGF (probably by the K4-SPH domain) and InlB (probably by $InlB_{321}$), as shown by FCS and biophysical methods.

generous gift from Prof. Niemann (University of Bielefeld, Germany). The antibiotics coumermycin A1 and novobiocin used in the regulated mammalian expression system were from Promega. Antibodies were used to detect human MET (D1C2; Cell Signaling Technology), phospho-MET (D26 Tyr1234/1235; Cell Signaling Technology), ERK (K-23; Santa Cruz Biotechnology), phospho-ERK (Phospho-p44/42 MAPK; Cell Signaling Technology), CD44v6 (BIWA; Bender), and alpha-tubulin (Sigma-Aldrich). The secondary antibodies were labeled with horseradish peroxidase (HRP, Dako) or Alexa 555 (Life Technologies). Methyl-β-cyclodextrin (MβCD, Sigma-Aldrich) was used to deplete cholesterol from the membrane.

4.2. Plasmids

The plasmid pF12A-MET-EGFP was previously cloned as explained in [16]. The vector pReg neo (pReg, Promega) was used to express the coumermycin A1-inducible λRep-GyrB-AD transcription activator. The plasmid pRP-CD44v6-mCherry, cloned by Vector Builder, encodes the sequence of human CD44v6 linked to a sequence encoding mCherry into a regular expression vector. The plasmid pCS2-CD44s-mCherry encodes the sequence of human CD44s linked to a sequence encoding mCherry into a pCS2+ vector. The plasmid mCherry-Mem was a gift from Catherine Berlot (Addgene plasmid # 55779; http://n2t.net/addgene:55779; RRID: Addgene_55,779). pcDNA3.1-mCherry (mCherry) encodes the sequence of mCherry cloned in a pcDNA3.1(+) vector. pEGFP-N1 was a gift from M.M. Nalaskowski (Universitätsklinikum Hamburg-Eppendorf). The truncated pRP-CD44v6delta-cyt-mCherry plasmid, cloned by VectorBuilder, encodes the sequence of a truncated version of CD44v6 lacking the cytoplasmic domain, linked to a sequence encoding mCherry at the carboxy-terminal end into a regular expression vector.

4.3. Cell culture

T-47D cells (ATCC® HTB-133™, Human Breast Cancer) were grown in RPMI 1640 medium, supplemented with 10 % FBS (Fetal Bovine Serum, Dominique Dutscher), in addition to penicillin (100 U/mL) and streptomycin (100 U/mL) (PS; Lonza). HeLa cell lines were grown in DMEM medium, supplemented with 10 % FBS and 1 % PS. Cells were cultured in a humid atmosphere with 5 % CO_2 at 37 °C.

4.4. Transfection

For Western blots, 2×10^5 T-47D cells were seeded in 6-well plates a day prior to transfection. 1.5 μg DNA were transfected per well. Overall, 0.5 μg of pRP-CD44v6-mCherry (CD44v6-mCherry), 0.5 μg of pF12A-MET-EGFP (MET-EGFP), and 0.5 μg of pReg neo (pReg) were mixed in 100 μL serum-free Opti-MEM. For control samples, 0.75 μg of pF12A-MET-EGFP and 0.75 μg of pReg were prepared in 100 μL serum-free Opti-MEM.

For microscopy experiments, 1×10^4 T-47D cells were seeded in an

8-well chambered cover glass (IBL Baustoff + Labor GmbH) one day before the transfection experiment. 0.3 μg DNA was transfected per well. For FLIM experiments, 0.1 μg of pReg, 0.1 μg of pF12A-MET-EGFP, and 0.1 μg of CD44v6-mCherry or 0.1 μg of pCS2-CD44s-mCherry (CD44s-mCherry) were mixed in 30 μL serum-free Opti-MEM. For these experiments, control samples were transfected with 0.3 μg of pEGFP-GPI or 0.15 μg of pF12A-MET-EGFP and 0.15 μg of pReg or 0.15 μg of pEGFP-GPI and 0.15 μg of CD44v6-mCherry. For FCS experiments, 0.15 μg of pF12A-MET-EGFP and 0.15 μg of pReg or 0.3 μg of CD44v6-mCherry or 0.3 μg of CD44s-mCherry or 0.3 μg of CD44v6delta cyt-mCherry were mixed in 30 μL serum-free Opti-MEM. For the MET/CD44v6 complex diffusion measurements by FCS, 0.1 μg of pReg, 0.1 μg of pF12A-MET-EGFP, and 0.1 μg of CD44v6-mCherry were mixed in 30 μL serum-free Opti-MEM. FCS control samples were transfected with 0.3 μg mCherry-Mem or pcDNA3.1-mCherry (mCherry) plasmids. MET fusion protein expression was induced as described in [16]. In brief, after 3 h of transfection, 0.8 nM coumermycin A1 was added to serum-starved cells, and then induction was stopped 6 h later by the addition of 5 μM of novobiocin to the cells.

For all experiments, Viafect (Promega) transfection reagent was added to the DNA mixture in a ratio of 3:1. The mixture was then incubated at room temperature (RT) for 10 min and added dropwise to the 6-well plates or the 8-well chambered cover glass. The transfection outcome was checked by fluorescence microscopy to adjust the time of incubation. During the acquisition, cells were maintained in Leibovitz L-15 Medium (Gibco) at 37 °C.

4.5. Cell treatment

For lipid studies, HeLa cells were seeded two days prior to treatment. After 24 h, growth medium was replaced by serum-free basal medium overnight to remove all growth factors of the FBS. On the next day, cells were incubated at 37 °C with the specific drugs in lipoprotein-deficient serum (LPDS) or serum-free medium, according to Table 1.

For the investigation of the actin cytoskeleton in the diffusion of CD44v6, T-47D cells were seeded three days before treatment, transfected as described in the chapter transfection on day 2, and incubated on day 3 with 5 μM of Cytochalasin D (Merck) and 0.5 μg/mL of Latrunculin A (Merck) for 5 min, before FCS measurements.

4.6. Induction of cells with HGF or InlB

For Western blot analysis, the cells were treated with 50 ng/mL HGF or InlB in serum-free medium for 5 min at 37 °C. They were then washed with cold PBS before cell lysis. For microscopy experiments, cells were incubated with 50 ng/mL of the ligands in L-15 medium for 10 min at 37 °C before measurements.

4.7. Fluorescence lifetime imaging microscopy

FLIM measurements were performed on a multi-photon confocal microscope. The setup was a homemade two-photon excitation scanning microscope based on an Olympus IX70 inverted microscope with a 60 × 1.2 NA water immersion objective and a thermostat (at 25 °C or 37 °C depending on the experiments [54]). The excitation source was provided by a broadband femtosecond laser 680–1300 nm (Insight DeepSee, Spectra Physics) that allows the excitation of most of the fluorescent dyes. The laser power is adjustable (between μW up to 100 mW) to optimize the parameters of acquisition. EGFP was excited at 930 nm. Fluorescence photons were collected in the descanned fluorescence collection mode using a short-pass filter with a cut-off wavelength of 680 nm (F75–680, AHF filter) and two fiber-coupled APD (SPCM-AQR-14-FC, PerkinElmer) in single photon counting mode. The photon signals were collected through a hardware correlator (ALV5000, ALV GmbH) connected to a time-correlated single photon counting (TCSPC) module (SPC830, Becker & Hickl) for FLIM measurements. To obtain appropriate photon counts, FLIM images were acquired between 90 and 240 s. The data were analyzed using the software SPCImage (v.8.5, Becker & Hickl) that fits the decay of each pixel with a binning of two to obtain >15,000 counts associated to each pixel to optimize the fit. The data were also analyzed with the FlimFIT software (v.5.1.1, Imperial College London).

Table 1
Drugs targeting different lipids.

Drugs	Concentration	Duration
Lovastatin (Tokyo chemical industry) in LPDS-DMEM	8 μM	18 h
U18666A (Enzo life sciences) in LPDS-DMEM	2 μg/mL	18 h
Bacterial Sphingomyelinase (Sigma-Aldrich) in serum-free DMEM	0.5 unit/mL	30 min
Desipramine hydrochloride (Sigma-Aldrich) in LPDS-DMEM	25 μM	2 h
ISP-1/Myriocin (Sigma-Aldrich) in LPDS-DMEM	3 μM	18 h
Methyl-β-cyclodextrin (MβCD) (Sigma-Aldrich) in serum-free DMEM	10–20 mM	30 min

4.8. Fluorescence correlation spectroscopy

FCS measurements were performed on the same two-photon microscope as described for FLIM. The fluorescence signal was collected with a hardware correlator (ALV5000, ALV GmbH) that generates on-line autocorrelation and cross-correlation curves for FCS measurements and a time-correlated single photon counting (TCSPC) module. EGFP was excited at 930 nm. Fluorescence photons were collected using a short-pass filter with a cut-off wavelength of 680 nm (F75–680) and a band-pass filter of 525/40 nm (F37–520) for EGFP. mCherry was excited at 1160 nm with a long-pass filter of 600/70 nm. The focal volume for EGFP was estimated by using as a reference a 50 nM solution of tetramethylrhodamine (TMR) with a known diffusion coefficient (D = 592 $\mu m^2/s$ at 37 °C; [55]) and for mCherry, ATTO 655 (D = 570 $\mu m^2/s$ at 37 °C; [56]) was used. For mCherry measurements, 40 acquisitions of 5 s duration were realized compared to 20 acquisitions of 10 s for EGFP measurements. Autocorrelation curves were calculated by a home-made Matlab program. The following 3D and 2D diffusion models were used for cytoplasmic proteins and membrane proteins, respectively.

(3D model)

$$G(\tau) = \frac{1}{N}\frac{1}{\left(1+\left(\frac{\tau}{\tau_D}\right)\right)}\frac{1}{\sqrt{1+\left(\frac{r_0}{Z_Z}\right)^2\left(\frac{\tau}{\tau_D}\right)}}$$

(2D model)

$$G(\tau) = \frac{1}{N}\frac{1}{\left(1+\left(\frac{\tau}{\tau_D}\right)\right)}$$

where N represents the mean number of fluorescent particles in the focal volume, while r_0 and Z_z correspond to the lateral and axial dimensions of the focal volume, respectively. τ_D corresponds to the transit time.

The diffusion coefficient of the proteins was calculated by:

$$D_{sample} = \frac{\tau_{reference}}{\tau_{sample}} \times D_{reference}$$

where $\tau_{reference}$ and $D_{reference}$ represent respectively the correlation time and the diffusion coefficient of TMR or ATTO 665.

Both the fluorescence brightness and the diffusion coefficient of fusion proteins can be measured using FCS [57]. After analysis using our custom Matlab program, the autocorrelation curves provided

information about the brightness and number of molecules. By comparing their relative brightness to the brightness of the fluorescence protein alone (EGFP or mCherry), one can infer the degree of protein oligomerization from their brightness.

This method was previously utilized by us to assess MET's oligomerization. Briefly, fluorescent proteins were produced in cells, and brightness (B) was evaluated by the formula B=Intensity signal/N, where N is the average number of fluorescent particles identified from each autocorrelation curve (Fig. 3). A monomeric distribution corresponds to a brightness of 0.50–1.50 after normalizing the obtained distributions of B values for EGFP and mCherry to one. We studied EGFP and EGFPx2 (a gift from Dr. M.M. Nalaskowski) to validate this strategy [58]. The brightness of EGFPx2 was found to be between 1.5 and 2.5, as predicted. We studied cytoplasmic EGFP and GPI-EGFP (a gift from Thorsten Wohland) to see if the location of the proteins in the membrane altered the brightness, but there was no discernible change. Proteins with B values between 0.5 and 1.5, 1.5 and 2.5, and $>$ 2.5 were, respectively, categorized as monomeric, dimeric, and trimeric or more using the outlined FCS technique.

4.9. Western blotting

Cells were lysed in 100 mM dithiothreitol containing SDS-sample buffer (125 mM TrisHCl pH 6.8; 4 % SDS; 20 % Glycerol; 0.01 % bromophenol blue). Cell lysates were then subjected to SDS-page and blotted to nitrocellulose membranes and probed with appropriate antibodies (listed in reagents). For loading controls, phosphorylated MET and phosphorylated ERK blots were stripped using a Western blot stripping buffer (Restore Plus, ThermoFisher), and reprobed with an anti-MET specific antibody and an anti-ERK specific antibody, respectively. Therefore, phosphorylated MET expression was compared to total MET level, while phosphorylated ERK expression was compared to total ERK level. On the other hand, the expression of CD44v6 was normalized by the housekeeping gene, alpha-tubulin. Detection of the antibodies was performed with the enhanced chemiluminescence detection kit (clarity Western blot ECL substrate) using Image Quant LAS-4000 imaging system (GE Healthcare). Blot densitometry analysis was carried out using Fiji software [59].

4.10. Immunofluorescence staining

Following treatment with MβCD, cells were induced or not with 50 ng/mL HGF at 37 °C. Cells were washed once with cold PBS and then fixed with cold methanol at −20 °C for 10 min. After fixation, cells were washed thrice with cold PBS and afterwards blocked with 3 % bovine serum albumin (BSA) in PBS at RT for 30 min. Then, the cells were incubated overnight with an antibody targeted against phosphorylated MET (diluted 1:500) at 4 °C. The next day, cells were washed three times with PBS, incubated with a goat anti-rabbit-Alexa 555 antibody (1:1000) for 30 min at RT washed another three times, and then incubated with 1 μg/mL of DAPI for 10 min in the dark at RT. Finally, the cells were washed three more times before the cover slips were mounted with antifade mounting medium (ProLong Diamond, Molecular Probes). The slides were left to dry at RT for 24 h. They were then imaged on confocal laser scanning microscope (LSM700, Zeiss) equipped with a Plan-Apochromat 63 × 1.40 oil immersion objective. Alexa fluor 555 was excited with a 555 nm laser and DAPI was excited with a 405 nm laser line. Images of 1024 px × 1024 px were processed by the Fiji software [59].

4.11. MicroScale thermophoresis

10 μM of K4-SPH, NK2, CD44s, or CD44v6 ectodomain were labeled with a red fluorescent dye (NT-647) using the Protein Labeling NHS RED Kit (NanoTemper Technologies). 10 μM of proteins were incubated with 30 μM of the fluorophore NT-647 for 30 min at RT protected from light. Meanwhile a gravity flow column was equilibrated with 10 mL PBS. After incubation, the labeled proteins were loaded on the gel filtration column to separate free dyes from labeled proteins. 10 nM of fluorescently labeled protein were added to a serial dilution of unlabeled proteins (CD44s or CD44v6 ectodomain, or $InlB_{321}$). The samples were loaded into hydrophilic capillaries (NanoTemper Technologies, reference K004). Measurements were performed in the Monolith NT.115 at 22 °C in PBS plus 1 % BSA by using 50 % LED power and 80 % IR-laser power. Data were analyzed using NanoTemper Analysis software v.1.4.23 and plotted using the OriginPro v.8.6 software from OriginLab. The NK2 and K4-SPH domains were a kind gift from a gift from Ermanno Gherardi, University of Pavia, Italy.

4.12. Statistical analysis

For FLIM and FCS experiments, at least 5 cells per condition and per experiment were measured and the quantification was performed from at least 5 independent experiments. All the tests were executed on a statistical analysis tool (GraphPad Prism version 8).

CRediT authorship contribution statement

Ryshtee Mary Tannoo: Conceptualization, Methodology, Investigation, Formal analysis, Visualization, Writing - Original Draft, Writing - Review & Editing. Ludovic Richert: Conceptualization, Methodology, Formal analysis, Supervision. David Koschut: Methodology, Investigation, Formal analysis. Nario Tomishige: Methodology, Formal analysis. Sven Máté Treffert: Investigation, Formal analysis. Toshihide Kobayashi: Methodology, Formal analysis, Resources. Yves Mély: Conceptualization, Supervision, Formal analysis, Writing - Original Draft, Writing - Review & Editing, Funding acquisition. Véronique Orian-Rousseau: Conceptualization, Supervision, Formal analysis, Writing - Original Draft, Writing - Review & Editing, Funding acquisition.

Declaration of competing interest

The authors declare the following financial interests/personal relationships which may be considered as potential competing interests:

Veronique Orian-Rousseau reports a relationship with Amcure that includes: board membership and equity or stocks. VOR is a founder of the start-up company Amcure. The research herein has no link to this company.

Data availability

Data will be made available on request.

Acknowledgements

We are thankful to Ermanno Gherardi (University of Pavia, Pavia, Italy) for providing HGF domains. Fig. 6 and the graphical abstract were created on Biorender.com. This work and R.M.T. were funded by the Deutsche Französische Hochschule (DFH), the international doctoral program of the European doctoral college of UNISTRA, and the doctoral school of life and sciences (ED 414) of UNISTRA. The PhD of RMT was a co-tutelle between UNISTRA and KIT. Support was obtained from the French National Centre for Scientific Research (CNRS) and the Hemholtz program Information - Materials Systems Engineering (MSE), Germany. Y. M. is grateful to the Institut Universitaire de France (IUF) for support and providing additional time to be dedicated to research. Imaging was supported by the Imaging Center PIQ-QuESt (https://piq.unistra.fr/).

Appendix A. Supplementary data

Supplementary data to this article can be found online at https://doi.org/10.1016/j.bbamem.2023.184236.

References

[1] C. Birchmeier, W. Birchmeier, E. Gherardi, G.F. Vande Woude, Met, metastasis, motility and more, Nat. Rev. Mol. Cell Biol. 4 (12) (Dec. 2003) 915–925, https://doi.org/10.1038/nrm1261.

[2] M. Borowiak, A.N. Garratt, T. Wüstefeld, M. Strehle, C. Trautwein, C. Birchmeier, Met provides essential signals for liver regeneration, Proc. Natl. Acad. Sci. 101 (29) (Jul. 2004) 10608–10613, https://doi.org/10.1073/pnas.0403412101.

[3] P.M. Comoglio, S. Giordano, L. Trusolino, Drug development of MET inhibitors: targeting oncogene addiction and expedience, Nat. Rev. Drug Discov. 7 (6) (Jun. 2008) 504–516, https://doi.org/10.1038/nrd2530.

[4] G. Viticchiè, P. Muller, C-met and other cell surface molecules: interaction, activation and functional consequences, Biomedicines 3 (1) (Jan. 2015) 46–70, https://doi.org/10.3390/biomedicines3010046.

[5] V. Orian-Rousseau, L. Chen, J. Sleeman, P. Herrlich, H. Ponta, CD44 is required for two consecutive steps in HGF/c-Met signaling, Genes Dev. 16 (23) (Dec. 2002) 3074–3086, https://doi.org/10.1101/gad.242602.

[6] V. Orian-Rousseau, J. Sleeman, CD44 is a multidomain signaling platform that integrates extracellular matrix cues with growth factor and cytokine signals, Advances in Cancer Research, Elsevier (2014) 231–254, https://doi.org/10.1016/B978-0-12-800092-2.00009-5.

[7] Y. Volz, et al., Direct binding of hepatocyte growth factor and vascular endothelial growth factor to CD44v6, Biosci. Rep. 35 (4) (2015), https://doi.org/10.1042/BSR20150093 e00236.

[8] A. Matzke-Ogi, et al., Inhibition of tumor growth and metastasis in pancreatic cancer models by interference with CD44v6 signaling, Gastroenterology 150 (2) (Feb. 2016), https://doi.org/10.1053/j.gastro.2015.10.020, pp. 513-525.e10.

[9] M. Hamon, H. Bierne, P. Cossart, Listeria monocytogenes: a multifaceted model, Nat. Rev. Microbiol. 4 (6) (Jun. 2006) 423–434, https://doi.org/10.1038/nrmicro1413.

[10] Y. Shen, M. Naujokas, M. Park, K. Ireton, InlB-dependent internalization of Listeria is mediated by the met receptor tyrosine kinase, Cell 103 (3) (2000) 501–510.

[11] C. Jung, A. Matzke, H.H. Niemann, C. Schwerk, T. Tenenbaum, V. Orian-Rousseau, Involvement of CD44v6 in InlB-dependent *Listeria* invasion, Mol. Microbiol. 72 (5) (Jun. 2009) 1196–1207, https://doi.org/10.1111/j.1365-2958.2009.06716.x.

[12] J. Schlessinger, Cell signaling by receptor tyrosine kinases, Cell 103 (2) (Oct. 2000) 211–225, https://doi.org/10.1016/S0092-8674(00)00114-8.

[13] M.A. Lemmon, J. Schlessinger, Cell signaling by receptor tyrosine kinases, Cell 141 (7) (Jun. 2010) 1117–1134, https://doi.org/10.1016/j.cell.2010.06.011.

[14] D.L. Wheeler, Y. Yarden, Receptor Tyrosine Kinases: Structure, Functions and Role in Human Disease, Springer New York, New York, NY, 2015, https://doi.org/10.1007/978-1-4939-2053-2.

[15] M.S. Dietz, D. Haße, D.M. Ferraris, A. Göhler, H.H. Niemann, M. Heilemann, Single-molecule photobleaching reveals increased MET receptor dimerization upon ligand binding in intact cells, BMC Biophys. 6 (1) (2013) 6, https://doi.org/10.1186/2046-1682-6-6.

[16] D. Koschut, L. Richert, G. Pace, H.H. Niemann, Y. Mély, V. Orian-Rousseau, Live cell imaging shows hepatocyte growth factor-induced Met dimerization, Biochim. Biophys. Acta BBA - Mol. Cell Res. 1863 (7) (Jul. 2016) 1552–1558, https://doi.org/10.1016/j.bbamcr.2016.04.015.

[17] E. Uchikawa, Z. Chen, G.-Y. Xiao, X. Zhang, X. Bai, Structural basis of the activation of c-MET receptor, Nat. Commun. 12 (1) (Dec. 2021) 4074, https://doi.org/10.1038/s41467-021-24367-3.

[18] N.A. Lokker, et al., Structure-function analysis of hepatocyte growth factor: identification of variants that lack mitogenic activity yet retain high affinity receptor binding, EMBO J. 11 (7) (Jul. 1992) 2503–2510, https://doi.org/10.1002/j.1460-2075.1992.tb05315.x.

[19] E. Gherardi, et al., Functional map and domain structure of MET, the product of the c-met protooncogene and receptor for hepatocyte growth factor/scatter factor, Proc. Natl. Acad. Sci. 100 (21) (2003) 12039–12044.

[20] E. Gherardi, et al., Structural basis of hepatocyte growth factor/scatter factor and MET signalling, Proc. Natl. Acad. Sci. 103 (11) (2006) 4046–4051.

[21] T. Kobayashi, M. Takahashi, Y. Nagatsuka, Y. Hirabayashi, Lipid rafts: new tools and a new component, Biol. Pharm. Bull. 29 (8) (2006) 1526–1531, https://doi.org/10.1248/bpb.29.1526.

[22] A. Pietraszewska-Bogiel, T.W.J. Gadella, FRET microscopy: from principle to routine technology in cell biology: FRET MICROSCOPY, J. Microsc. 241 (2) (Feb. 2011) 111–118, https://doi.org/10.1111/j.1365-2818.2010.03437.x.

[23] S. Pelet, M.J.R. Previte, P.T.C. So, Comparing the quantification of Förster resonance energy transfer measurement accuracies based on intensity, spectral, and lifetime imaging, J. Biomed. Opt. 11 (3) (2006), https://doi.org/10.1117/1.2203664, p. 034017.

[24] L. Beviglia, K. Matsumoto, C.-S. Lin, B.L. Ziober, R.H. Kramer, Expression of the C-Met/HGF Receptor in Human Breast Carcinoma: Correlation with Tumor Progression, 1997, p. 9.

[25] Y. Han, Y. Luo, J. Zhao, M. Li, Y. Jiang, Overexpression of c-met increases the tumor invasion of human prostate LNCaP cancer cells in vitro and in vivo, Oncol. Lett. 8 (4) (Oct. 2014) 1618–1624, https://doi.org/10.3892/ol.2014.2390.

[26] H.-F. Zhao, J. Boyd, N. Jolicoeur, S.-H. Shen, A coumermycin/Novobiocin-regulated gene expression system, Hum. Gene Ther. 14 (17) (Nov. 2003) 1619–1629, https://doi.org/10.1089/104303403322542266.

[27] M.-L.I.E. Harwardt, et al., Single-molecule super-resolution microscopy reveals heteromeric complexes of MET and EGFR upon ligand activation, Int. J. Mol. Sci. 21 (8) (Apr. 2020) 2803, https://doi.org/10.3390/ijms21082803.

[28] T.N. Baldering, et al., CRISPR/Cas12a-mediated labeling of MET receptor enables quantitative single-molecule imaging of endogenous protein organization and dynamics, iScience 24 (1) (Jan. 2021), https://doi.org/10.1016/j.isci.2020.101895, 101895.

[29] J.V. Fritz, et al., Direct Vpr-Vpr interaction in cells monitored by two photon fluorescence correlation spectroscopy and fluorescence lifetime imaging, Retrovirology 5 (1) (2008) 87, https://doi.org/10.1186/1742-4690-5-87.

[30] B. Ilien, et al., Pirenzepine promotes the dimerization of muscarinic M1 receptors through a three-step binding process, J. Biol. Chem. 284 (29) (Jul. 2009) 19533–19543, https://doi.org/10.1074/jbc.M109.017145.

[31] D.S. Lidke, et al., ERK nuclear translocation is dimerization-independent but controlled by the rate of phosphorylation, J. Biol. Chem. 285 (5) (Jan. 2010) 3092–3102, https://doi.org/10.1074/jbc.M109.064972.

[32] M.-L.I.E. Harwardt, et al., Membrane dynamics of resting and internalin B-bound MET receptor tyrosine kinase studied by single-molecule tracking, FEBS Open Bio 7 (9) (Sep. 2017) 1422–1440, https://doi.org/10.1002/2211-5463.12285.

[33] N. Dross, C. Spriet, M. Zwerger, G. Müller, W. Waldeck, J. Langowski, Mapping eGFP oligomer mobility in living cell nuclei, PLoS ONE 4 (4) (Apr. 2009), https://doi.org/10.1371/journal.pone.0005041 p. e5041.

[34] K. AbuZineh, L.I. Joudeh, B. Al Alwan, S.M. Hamdan, J.S. Merzaban, S. Habuchi, Microfluidics-based super-resolution microscopy enables nanoscopic characterization of blood stem cell rolling, Sci. Adv. 4 (7) (Jul. 2018), https://doi.org/10.1126/sciadv.aat5304 p. eaat5304.

[35] T. Murai, Y. Maruyama, K. Mio, H. Nishiyama, M. Suga, C. Sato, Low cholesterol triggers membrane microdomain-dependent CD44 shedding and suppresses tumor cell migration, J. Biol. Chem. 286 (3) (Jan. 2011) 1999–2007, https://doi.org/10.1074/jbc.M110.184010.

[36] V. Kilin, O. Glushonkov, L. Herdly, A. Klymchenko, L. Richert, Y. Mely, Fluorescence lifetime imaging of membrane lipid order with a Ratiometric fluorescent probe, Biophys. J. 108 (10) (May 2015) 2521–2531, https://doi.org/10.1016/j.bpj.2015.04.003.

[37] V. Orian-Rousseau, et al., Hepatocyte growth factor-induced Ras activation requires ERM proteins linked to both CD44v6 and F-actin, Mol. Biol. Cell 18 (1) (Jan. 2007) 76–83, https://doi.org/10.1091/mbc.e06-08-0674.

[38] D.E. Hammond, S. Urbé, G.F. Vande Woude, M.J. Clague, Down-regulation of MET, the receptor for hepatocyte growth factor, Oncogene 20 (22) (May 2001) 2761–2770, https://doi.org/10.1038/sj.onc.1204475.

[39] A. Duriatti, et al., In vitro inhibition of animal and higher plants 2,3-oxidosqualene-sterol cyclases by 2-aza-2,3- dihydrosqualene and derivatives, and by other ammonium-containing molecules, Biochem. Pharmacol. 34 (15) (Aug. 1985) 2765–2777, https://doi.org/10.1016/0006-2952(85)90578-7.

[40] L. Liscum, J.R. Faust, The intracellular transport of low density lipoprotein-derived cholesterol is inhibited in Chinese hamster ovary cells cultured with 3-β-[2-(diethylamino)ethoxy]androst-5-en-17-one, J. Biol. Chem. 264 (20) (Jul. 1989) 11796–11806, https://doi.org/10.1016/S0021-9258(18)80136-3.

[41] R. Ishitsuka, T. Saito, H. Osada, Y. Ohno-Iwashita, T. Kobayashi, Fluorescence image screening for chemical compounds modifying cholesterol metabolism and distribution, J. Lipid Res. 52 (11) (Nov. 2011) 2084–2094, https://doi.org/10.1194/jlr.D018184.

[42] G.C. Carter, L. Bernstone, D. Sangani, J.W. Bee, T. Harder, W. James, HIV entry in macrophages is dependent on intact lipid rafts, Virology 386 (1) (Mar. 2009) 192–202, https://doi.org/10.1016/j.virol.2008.12.031.

[43] S. Nakamura, Y. Kozutsumi, Y. Sun, Y. Miyake, T. Fujita, T. Kawasaki, Dual roles of sphingolipids in signaling of the escape from and onset of apoptosis in a mouse cytotoxic T-cell line, CTLL-2 (*), J. Biol. Chem. 271 (3) (Jan. 1996) 1255–1257, https://doi.org/10.1074/jbc.271.3.1255.

[44] P. Papatheodorou, C. Zamboglou, S. Genisyuerek, G. Guttenberg, K. Aktories, Clostridial glucosylating toxins enter cells via clathrin-mediated endocytosis, PloS One 5 (5) (May 2010), https://doi.org/10.1371/journal.pone.0010673 p. e10673.

[45] S. Albouz, F. Le Saux, D. Wenger, J.J. Hauw, N. Baumann, Modifications of sphingomyelin and phosphatidylcholine metabolism by tricyclic antidepressants and phenothiazines, Life Sci. 38 (4) (Jan. 1986) 357–363, https://doi.org/10.1016/0024-3205(86)90083-4.

[46] N.K. Karamanos, et al., A guide to the composition and functions of the extracellular matrix, FEBS J. 288 (24) (Dec. 2021) 6850–6912, https://doi.org/10.1111/febs.15776.

[47] A.R. Vega, S.A. Freeman, S. Grinstein, K. Jaqaman, Multistep track segmentation and motion classification for transient mobility analysis, Biophys. J. 114 (5) (Mar. 2018) 1018–1025, https://doi.org/10.1016/j.bpj.2018.01.012.

[48] S.A. Freeman, et al., Transmembrane pickets connect cyto- and pericellular skeletons forming barriers to receptor engagement, Cell 172 (1–2) (Jan. 2018), https://doi.org/10.1016/j.cell.2017.12.023, pp. 305–317.e10.

[49] S. Mylvaganam, et al., Stabilization of endothelial receptor arrays by a polarized spectrin cytoskeleton facilitates rolling and adhesion of leukocytes, Cell Rep. 31 (12) (Jun. 2020), https://doi.org/10.1016/j.celrep.2020.107798, 107798.

[50] P. Sil, et al., Dynamic actin-mediated nano-scale clustering of CD44 regulates its meso-scale organization at the plasma membrane, Mol. Biol. Cell 31 (7) (Mar. 2020) 561–579, https://doi.org/10.1091/mbc.E18-11-0715.

[51] S. Hasenauer, et al., Internalization of Met requires the co-receptor CD44v6 and its link to ERM proteins, PLoS ONE 8 (4) (Apr. 2013), https://doi.org/10.1371/journal.pone.0062357 p. e62357.

[52] K.-L. Chen, D. Li, T.-X. Lu, S.-W. Chang, Structural characterization of the CD44 stem region for standard and cancer-associated isoforms, Int. J. Mol. Sci. 21 (1) (Jan. 2020) 336, https://doi.org/10.3390/ijms21010336.

[53] M. Ebbes, W.M. Bleymüller, M. Cernescu, R. Nölker, B. Brutschy, H.H. Niemann, Fold and function of the InlB B-repeat, J. Biol. Chem. 286 (17) (Apr. 2011) 15496–15506, https://doi.org/10.1074/jbc.M110.189951.

[54] J.P. Clamme, J. Azoulay, Y. Mély, Monitoring of the formation and dissociation of Polyethylenimine/DNA complexes by two photon fluorescence correlation spectroscopy, Biophys. J. 84 (3) (Mar. 2003) 1960–1968, https://doi.org/10.1016/S0006-3495(03)75004-8.
[55] T. Dertinger, V. Pacheco, I. von der Hocht, R. Hartmann, I. Gregor, J. Enderlein, Two-focus fluorescence correlation spectroscopy: a new tool for accurate and absolute diffusion measurements, ChemPhysChem 8 (3) (2007) 433–443, https://doi.org/10.1002/cphc.200600638.
[56] T. Dertinger, I. von der Hocht, A. Loman, R. Erdmann, J. Enderlein, Latest applications for 2-focus fluorescence correlation spectroscopy, in: Single Molecule Spectroscopy and Imaging, SPIE, 2008, 686202, https://doi.org/10.1117/12.762365.
[57] Y. Chen, J.D. Müller, Q. Ruan, E. Gratton, Molecular brightness characterization of EGFP in vivo by fluorescence fluctuation spectroscopy, Biophys. J. 82 (1) (Jan. 2002) 133–144, https://doi.org/10.1016/S0006-3495(02)75380-0.
[58] N.M. Seibel, J. Eljouni, M.M. Nalaskowski, W. Hampe, Nuclear localization of enhanced green fluorescent protein homomultimers, Anal. Biochem. 368 (1) (Sep. 2007) 95–99, https://doi.org/10.1016/j.ab.2007.05.025.
[59] J. Schindelin, et al., Fiji: an open-source platform for biological-image analysis, Nat. Methods 9 (7) (Jul. 2012) 676–682, https://doi.org/10.1038/nmeth.2019.